

Fabry-Pérot transmission resonances in tunneling microscopy

J. A. Kubby, Y. R. Wang, and W. J. Greene

Xerox Webster Research Center, Webster, New York 14580

(Received 14 September 1990; revised manuscript received 18 January 1991)

We have used the tunneling microscope to observe stacking-fault contrast in conductance and topographic images of the Si(111)- 7×7 surface as a function of applied gap bias. This contrast is found to be a strong function of the bias, with the maximal contrast occurring near energies where standing-wave formation, between the surface and a buried interface, is predicted in a one-dimensional resonant-tunneling theory. The agreement between experiment and theory indicates that this technique is useful for probing details of buried interfaces formed by surface reconstruction and in heteroepitaxial growth.

An important structural aspect of the Si(111)- 7×7 reconstruction in the dimer-adtom-stacking-fault (DAS) model proposed by Takayanagi *et al.*¹ is the existence of a subsurface stacking fault in one half of the diamond-shaped unit cell. This fault gives rise to an asymmetry in the electronic properties of the unit cell that have been detected with the tunneling microscope under various biasing conditions.²⁻⁷ These asymmetries include a Fermi-level state at ± 0.15 -eV tip bias^{6,7} that gives rise to a height asymmetry at positive-tip bias voltages,^{2,6} an adatom T_4 backbonding state^{4,5,7} at -1.5 eV that is slightly shifted in energy between the faulted and unfaulted halves of the unit cell⁴ giving rise to an observable height asymmetry around -1.5 -eV bias, and a stacking fault state⁴ over the faulted half of the unit cell at -2.8 eV that gives rise to an asymmetry in conductivity mappings at -2.0 eV. We have used the tunneling microscope to probe locally the differential and total tunneling conductance of the Si(111)- 7×7 surface as a function of bias between -0.25 and -10.0 eV and have found that the differential-conductivity contrast is oscillatory in bias about the short diagonal of the unit cell. In particular, the differential-conductivity oscillations are found to bracket states at -0.20 -, -2.8 -, and -7.8 -eV bias that gives rise to a height asymmetry between the two halves of the unit cell, indicating an increased state density over the faulted half of the unit cell at these tip biases. We have found that these states can be predicted in a one-dimensional model of resonant tunneling between the sample surface potential and a buried potential barrier that is spatially inhomogeneous due to the stacking fault. By variation of a single parameter, the depth of the stacking fault below the surface, we are able to fit three "particle in a box" type states to those found experimentally. This model ties together the previous observations of the Fermi-level state^{6,7} at -0.15 -eV tip bias, the conductivity contrast at -2.0 -eV (Ref. 4) bias, the extra state density found over the faulted half of the unit cell at -2.8 -eV bias,⁴ and leads to the prediction of a new state at -7.8 eV that has been experimentally observed. In addition, fitting the three experimentally determined states to the results of the one-dimensional model yields a reasonable value of 4.9 Å for the depth of the buried stacking fault below the surface.

The sample was cut from an arsenic-doped, 0.005 - Ω -cm Si(111) wafer, and prepared *ex situ* with a thin pas-

sivating oxide. The oxide was sublimated *in situ* at a sample temperature of 875°C by passing a direct current through the well outgassed specimen. The operation of the microscope to obtain conductivity maps has been described previously,^{4,8} so that it will only be described briefly here. We collect a tunneling topograph and a conductivity map simultaneously by superimposing a small (0.1 V) ac signal at 4.5 kHz on the dc bias of the vacuum gap, and detect the in phase ac component of the tunneling current with a lock-in amplifier.

Figure 1 shows a series of topographic (I) and conductance (II) images that were taken at different biases tunneling into the empty states of the Si(111)- 7×7 surface. Each image pair [(I) and (II)] was collected simultaneously. The data in Fig. 1(d), taken at a tip bias of -2.0 eV and a demanded tunneling current of 1 nA, correspond to the conditions used in the first study of stacking-fault-conductivity contrast by Becker *et al.*⁴ and the data are similar. The conductivity image shows contrast between the two halves of the unit cell; one equilateral triangle appears lighter than the other, indicating that it is an area of higher conductance. Becker *et al.*⁴ associated this conductivity contrast with the different substructures of the two halves of the unit mesh. In the DAS model proposed by Takayanagi *et al.*,¹ the outermost complete double layer in the unit mesh consists of two triangular subunits that are respectively faulted and unfaulted with respect to the substrate. The high-conductivity (bright) triangles pointing towards the right-hand side in Fig. 1(d) correspond to the faulted half⁴ of the unit cell at this bias. From the sequence of images in Fig. 1, it can be seen that at some biases, -0.25 eV (a), -2.0 eV (d), and -3.5 eV (f), the stacking-fault contrast is apparent; while at other biases, -1.0 eV (b), -1.5 eV (c), -2.5 eV (e), and -4.5 eV (g), this contrast is minimal, with the conductivity image rendering a reverse image of the topograph⁹ that is uniform across the two halves of the unit cell. In addition to these biases, similar stacking-fault contrast has been observed at -0.05 , -7.5 , and -8.0 eV, but these data are not shown in Fig. 1. At -0.05 eV, the topographic image is distorted due to the small gap width at this bias; whereas beyond -5.0 eV, the topographic images degrade due to a decreasing signal-to-noise ratio with increasing gap width. From the sequence of images shown in Fig. 1, it can also be seen that the phase of the

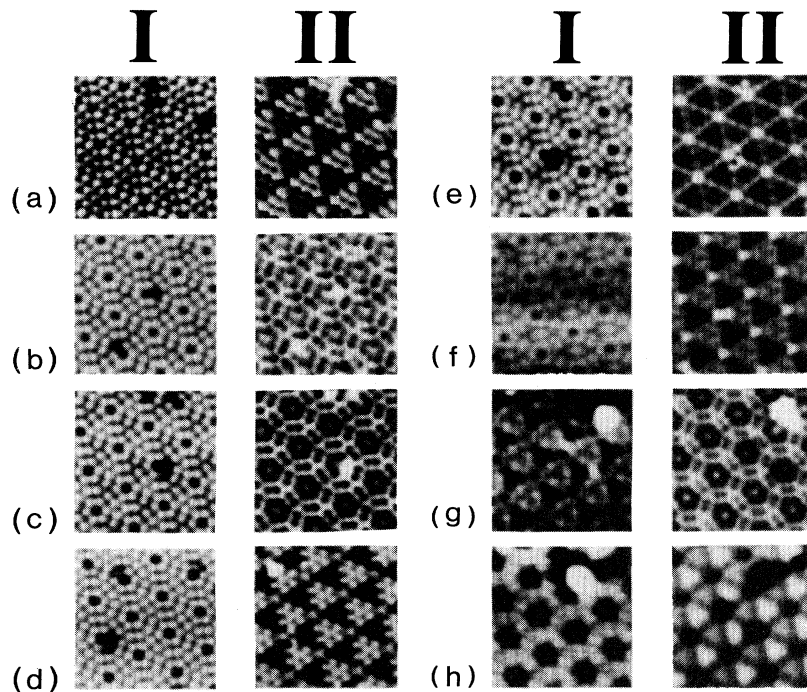


FIG. 1. Tunneling (I) and conductivity (II) images of the unoccupied states of Si(111)-7 \times 7 as a function of applied tip voltage. The gray scale range for the topograph is also indicated. (a) -0.25 eV (1.0 Å), (b) -1.0 eV (1.2 Å), (c) -1.5 eV (1.0 Å), (d) -2.0 eV (0.8 Å), (e) -2.5 eV (0.5 Å), (f) -3.5 eV (0.5 Å), (g) -4.5 eV (0.2 Å), and (h) -5.0 eV (0.2 Å). All images were acquired at a demanded tunneling current of 1 nA.

stacking-fault contrast in the conductivity images oscillates between the two halves of the unit cell as the applied bias is increased. The biases at which these phase reversals occur can be grouped into pairs: [-0.05 , -0.25 eV (a)], [-2.0 eV (d), -3.5 eV (f)], and [-7.5 , -8.0 eV]; where at the first bias the high-conductivity triangle points to the right-hand side (faulted half of the unit cell), and at the second bias it points to the left-hand side (unfaulted half). Between these phase oscillations in the conductivity images, the topographic image renders stacking-fault contrast as an apparent increase in height over the faulted half of the unit cell. Such contrast can be seen in the topographic images at -0.25 (a) and -2.50 eV (e), where the faulted half of the unit cell is 0.2 Å higher than the unfaulted half. Stacking-fault contrast can also be seen in the topographic images at -1.5 (c) and -4.50 eV (g) where the unfaulted half of the unit cell is 0.1 Å higher than the faulted half; however, the images at these biases are not bracketed by a phase reversal in the conductivity maps as found above and may be associated with a different phenomenon as discussed below. To test if the contrast oscillations associated with the stacking fault in Fig. 1 could arise from standing-wave formation between the sample surface at $Z=0$ and a buried interface at Z_0 , labeled as $n=1, 2$, and 3 in Fig. 2, we have calculated the conductivity for this one-dimensional potential.

The six parameters that enter into this model are the work functions of the tip and sample, the effective tunneling area, the Fermi energy of the tip, the strength of the δ -function scattering potential V_i , and its depth below the

surface Z_0 . To justify the use of this simple model, it is worthwhile to consider the influence of each of these parameters on the theoretical results. As we are measuring and calculating unoccupied states of the sample, the tip's electronic properties have little influence on the results.¹⁰ We have chosen values of $\phi_T=3.5$ eV and $\phi_S=3.1$ eV to

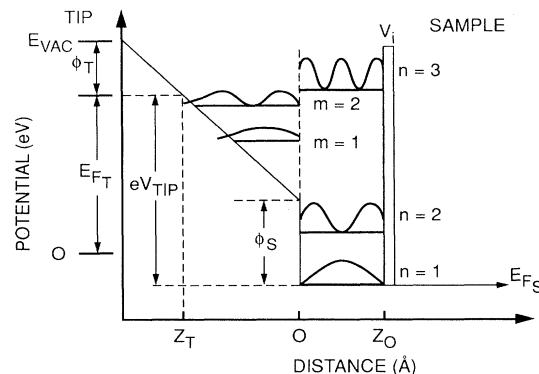


FIG. 2. Potential-energy diagram used in the calculations. The standing-wave resonances excited outside of the sample, between the surface and the classical turning point Z_T , have been labeled $m=1$ and 2 . The calculated electron probability densities $\psi^*\psi$, corresponding to standing-wave formation between the sample surface and buried interface at Z_0 , have been labeled $n=1, 2$, and 3 . The energy levels of the standing waves have been indicated by heavy lines under the electron probability densities.

place the first standing-wave peak, labeled $m=1$ in Fig. 2, at -5 eV as found in the experimental conductivity curves. The reduction of these values from the typical values for the work functions reflects the reduced barrier heights found in tunneling microscopy.¹¹ The effective tunneling area influences the initial gap width and hence the number of standing-wave peaks in a given bias interval. The value of 200 \AA^2 has been chosen to allow the formation of the $m=1-4$ standing-wave peaks in the bias interval from -5 to -10 eV as found in the experimental data. For the Fermi energy of the tip, we have used a typical value of 8 eV. The δ -function strength and its position are variables in the present model and have been labeled V_i and Z_0 , respectively, in the potential energy diagram shown in Fig. 2.

Figure 3 shows our calculated differential conductivity as a function of the applied gap bias for a constant demanded tunneling current of 1 nA. The tip trajectory calculated for this bias path is in excellent agreement with that found experimentally. An oscillatory behavior of the conductivity beyond a gap bias of -5 eV is obtained for $V_i=0$ in Fig. 3(a) as has been reported previously in association with electron standing-wave formation.^{4,8,12} Here each successive oscillation in dI/dV incorporates an additional standing wave in the gap, labeled as $m=1, 2$ in Fig. 2. When the interface δ -function strength increases, new structure appears in the conductivity spectrum that has

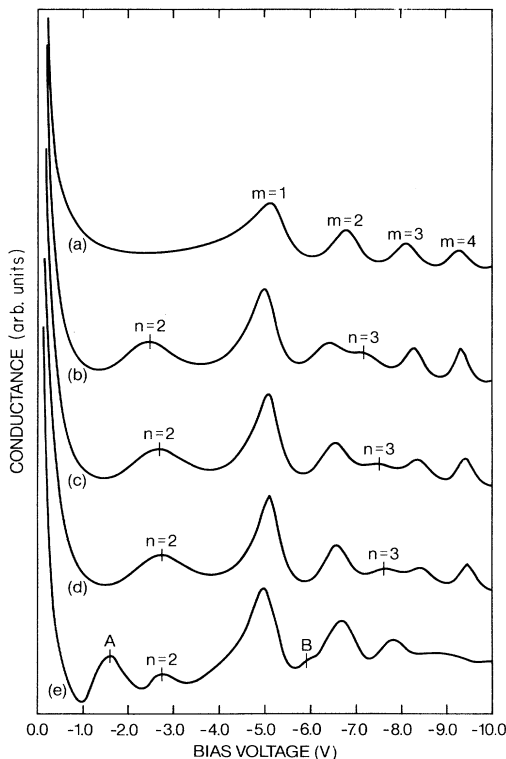


FIG. 3. Calculated conductance spectra vs V_{bias} for (a) $V_i=0$, (b) $V_i=1.5 \text{ eV \AA}$, $Z_0=5.2 \text{ \AA}$, (c) $V_i=1.5 \text{ eV \AA}$, $Z_0=5.0 \text{ \AA}$, (d) $V_i=1.5 \text{ eV \AA}$, $Z_0=4.9 \text{ \AA}$, and (e) experimental spectrum over the faulted half of the unit cell for a demanded tunneling current of 1 nA.

been labeled as $n=2$ and 3 in Fig. 3(b). This spectrum corresponds to values of $V_i=1.5 \text{ eV \AA}$ and $Z_0=5.2 \text{ \AA}$. The value of 1.5 eV \AA has been selected as it represents a value beyond the 1-eV-\AA threshold for obtaining the additional peaks, as discussed below. The depth of the scattering potential of 5.2 \AA has been chosen to represent the theoretically determined value for the depth at which the symmetry of the bulk crystal ends on the faulted half of the unit cell at the second bilayer into the solid. To derive this value, we have added together the height of the adatoms above the first bilayer,¹³ 1.7 \AA , one half the width of a bilayer, 0.4 \AA , and an interatomic spacing of 3.1 \AA . On the unfaulted side of the unit cell, the symmetry of the bulk crystal continues up to the first bilayer. In Fig. 3(b), we have identified the new peaks as the $n=2$ (-2.5 eV) and $n=3$ (-7.1 eV) standing waves by examining the electron probability density $\psi^*\psi$ between the surface at $Z=0$ and the buried interface at $Z=Z_0$. The electron probability density is plotted in Fig. 2. In addition, by examining $\psi^*\psi$ at low bias, we have been able to identify the $n=1$ standing-wave state at -0.2 eV. This peak is lost in the conductivity spectrum due to the large increase in conductivity as the bias approaches zero. The conductivity spectrum is calculated for $V_i=1.5 \text{ eV \AA}$ and $Z_0=5.0 \text{ \AA}$ in Fig. 3 to show the shift in the standing-wave peaks with a shift in the scattering-potential depth. The $n=2$ peak has shifted up to -2.7 eV, and the $n=3$ peak has increased to -7.5 eV; the calculated values scale almost as $(n/Z_0)^2$. In Fig. 3(d), the conductivity spectrum is calculated for $V_i=1.5 \text{ eV \AA}$ and $Z_0=4.9 \text{ \AA}$ in order to match the $n=2$ (-2.8 eV) standing-wave peak to the peak found at -2.8 eV in the experimental spectrum shown in Fig. 3(e). The $n=3$ peak in Fig. 3(d) has shifted up to -7.7 eV. The experimental spectrum 3(e) has additional structure, labeled *A* at -1.6 eV and *B* at -6.0 eV, which does not appear in the theoretical curve. Unlike the peak at -2.8 eV, which is localized to the faulted half of the unit cell,⁴ the structures at -1.5 and -6.0 eV are found on both sides of the unit cell⁴ and thus are not predicted by this theory as discussed below. The $n=3$ peak has not been labeled in the experimental spectrum as it is not clearly discernible from the $m=3$ state. We have, nonetheless, been able to detect the $n=3$ state near -7.8 eV bias due to its spatial contrast in conductivity maps.

We have also calculated conductivity spectra for various δ -function strengths in the range of 1 to 4 eV \AA . Beyond a threshold strength of 1 eV \AA necessary to obtain the additional structure, the peak positions remain stationary and only grow in magnitude with increasing scattering strength. Thus the peak positions are independent of the δ -function strength V_i over a wide range of strengths, whereas they vary almost as $(n/Z_0)^2$ with the scattering potential depth Z_0 .

The connection between the predictions of standing-wave formation in the one-dimensional resonant-tunneling theory, and the experimental observations of stacking-fault contrast in the topographic and differential conductivity images can be seen by consideration of the conductivity peak $n=2$ in Fig. 3(e). This peak is similar in energy to the -2.8 -eV peak in conductivity that was found to be localized over the faulted half of the unit cell by Becker

*et al.*⁴ Just below this peak, at -2.0 eV, the topographic image in Fig. 1(d) is uniform between the two halves of the unit cell, whereas the differential conductivity image II shows that the conductivity is increasing with bias on the faulted (bright) side of the unit cell. This increase in conductivity can be associated with an increase in the density of states with an incremental increase in bias, or an enhancement in the transmission coefficient with a change in bias. Examination of the theoretical results indicate that both effects are occurring. As the bias increases towards -2.8 eV, an increased density of final states becomes available over the faulted half of the unit cell in association with the formation of the $n=2$ standing wave shown in Fig. 2. Also, as the resonant condition is approached, the tunnel-barrier penetration probability is increasing. At resonance, in Fig. 1(e), the topographic image I renders stacking-fault contrast where the faulted half of the unit cell is high indicating an increased density of states over the faulted half of the unit cell.¹⁴ At this bias, the theory predicts extra final-state density on the faulted half of the unit cell from the excitation of the $n=2$ standing wave. The stacking fault contrast is minimal in the conductivity image at this bias as the tip follows contours of constant local density states.¹⁴ To first order, the tunneling microscope will act to nullify density of state contrast in differential conductance images through compensation in the tunnel gap width. As the barrier resonance at -2.8 eV falls below the source injection bias at -3.5 eV in Fig. 1(f), the stacking-fault contrast in the differential conductivity appears with reverse phase (stacking-fault dark), indicating a decrease of state density and barrier penetration probability over the faulted area with an incremental increase in bias. The topographic image once again becomes uniform over the two halves of the unit cell. In addition to the agreement between stacking-fault contrast predicted by the resonant-tunneling model and the stacking-fault contrast observed previously at -2 eV by Becker *et al.*,⁴ the theory also predicts stacking-fault contrast associated with the formation of the $n=1$ barrier resonance near -0.20 eV,^{6,7} and with the $n=3$ resonance near -7.7 eV. As mentioned previously, we have also observed topographic stacking-fault contrast with phase oscillation in the conductivity images that are bracketed by the bias pairs of $(-0.05, -0.25$ eV) and $(-7.5, -8.0$ eV) corresponding to the formation of the $n=1$ and 3 standing-wave states, respectively.

Finally, we consider the additional features labeled *A* and *B* in the experimental conductivity spectrum that are not predicted by the resonant-tunneling theory. Feature *A* in Fig. 3(d) occurs at -1.6 eV, and a small amount of stacking-fault contrast can be seen in the topographic image at -1.5 eV shown in Fig. 1(c). As shown by Becker *et al.*,⁴ this feature appears on both sides of the unit cell in the conductivity spectra; however, it is shifted down by 0.3 to -1.3 eV on the unfaulted half. This 0.3 -eV difference in the density-of-states maxima on either side of the unit cell would give rise to the stacking-fault contrast seen in Fig. 1(c). As this peak occurs on both halves of the unit cell, it is not explained by the theory presented here. The feature at -6.0 eV, labeled *B* in the experimental conductivity spectrum, can also be seen to be present on both halves of the surface unit cell in the data of Becker *et al.*⁴ We attribute this feature, and the contrast in the conductivity map in Fig. 1(h), to the formation of the $n=1$ standing-wave state within the adatom layer. This feature grows in strength when either tin or germanium is substituted for the silicon adatoms in T_4 sites.¹⁵ Application of the resonant-tunneling theory leads to a scattering depth of 1.5 Å for the formation of this state, which is in good agreement with theoretical adsorption heights for T_4 adatoms.¹³

In conclusion, we have observed stacking-fault contrast in topographic and differential-conductivity images of the Si(111)- 7×7 surface as a function of applied gap bias. The biases at which this contrast appears shows good agreement to biases at which a one-dimensional model of resonant tunneling predicts the formation of standing-wave solutions to the Schrödinger equation between scattering potentials located at the sample surface and at a buried interface. The agreement between experiment and theory demonstrates that electron standing-wave spectra, in conjunction with bias-dependent topographic and conductivity images, are useful for probing details of buried interfaces formed by surface reconstruction and in heteroepitaxial growth.¹⁵

We would like to acknowledge helpful discussions with R. S. Becker and C. B. Duke, and R. S. Becker and B. S. Swartzentruber for sharing their computer codes. We would also like to thank L. C. Pizzo for help in preparing the manuscript, and L. A. DeLouise and T. E. Orlowski for useful comments.

- ¹K. Takayanagi, Y. Tanishiro, M. Takahashi, and S. Takahashi, *J. Vac. Sci. Technol. A* **3**, 1502 (1985).
²G. Binnig, H. Rohrer, Ch. Gerber, and E. Weibel, *Phys. Rev. Lett.* **50**, 120 (1983).
³R. S. Becker, J. A. Golovchenko, E. G. McRae, and B. S. Swartzentruber, *Phys. Rev. Lett.* **55**, 2028 (1985).
⁴R. S. Becker, J. A. Golovchenko, D. R. Hamann, and B. S. Swartzentruber, *Phys. Rev. Lett.* **55**, 2032 (1985).
⁵R. J. Hamers, R. M. Tromp, and J. E. Demuth, *Phys. Rev. Lett.* **56**, 1972 (1986).
⁶R. M. Tromp, R. J. Hamers, and J. E. Demuth, *Phys. Rev. B* **34**, 1388 (1986).
⁷R. J. Hamers, R. M. Tromp, and J. E. Demuth, *Surf. Sci.* **181**,

346 (1987).

- ⁸R. S. Becker, J. A. Golovchenko, and B. S. Swartzentruber, *Phys. Rev. Lett.* **55**, 987 (1985).
⁹G. Binnig and H. Rohrer, *IBM J. Res. Dev.* **30**, 355 (1986).
¹⁰T. Klitsner, R. S. Becker, and J. S. Vickers, *Phys. Rev. B* **41**, 3837 (1990).
¹¹N. D. Lang, *Phys. Rev. B* **37**, 10395 (1988).
¹²G. Binnig and H. Rohrer, *Helv. Phys. Acta.* **55**, 726 (1982).
¹³J. E. Northrup, *Phys. Rev. Lett.* **57**, 154 (1986).
¹⁴J. Tersoff and D. R. Hamann, *Phys. Rev. B* **31**, 805 (1985).
¹⁵J. A. Kubby, Y. R. Wang, and W. J. Greene, *Phys. Rev. Lett.* **65**, 2165 (1990).

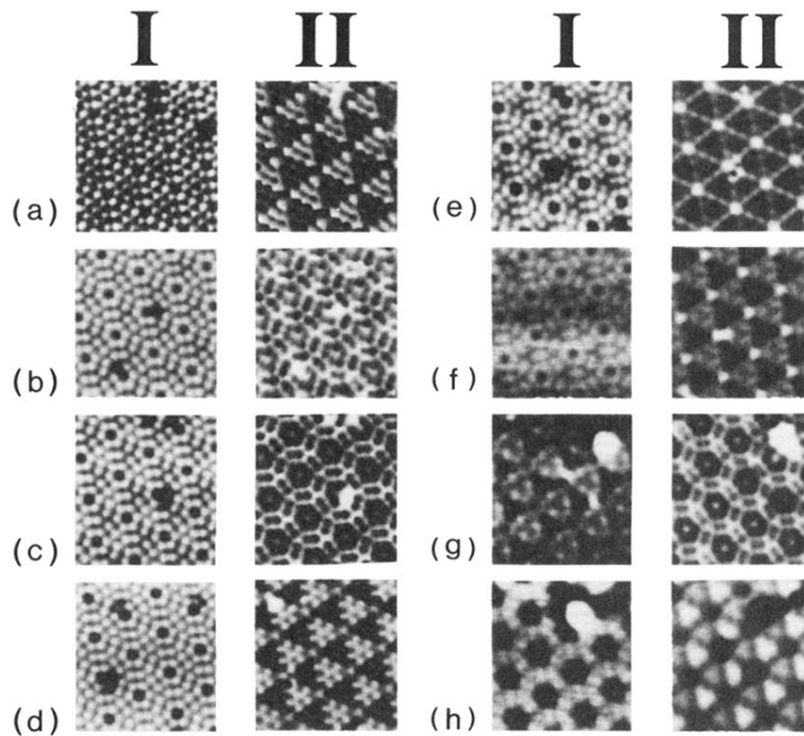


FIG. 1. Tunneling (I) and conductivity (II) images of the unoccupied states of Si(111)- 7×7 as a function of applied tip voltage. The gray scale range for the topograph is also indicated. (a) -0.25 eV (1.0 Å), (b) -1.0 eV (1.2 Å), (c) -1.5 eV (1.0 Å), (d) -2.0 eV (0.8 Å), (e) -2.5 eV (0.5 Å), (f) -3.5 eV (0.5 Å), (g) -4.5 eV (0.2 Å), and (h) -5.0 eV (0.2 Å). All images were acquired at a demanded tunneling current of 1 nA.